

Review

Applications of Nanomaterials for Theranostics of Melanoma

Guanqiao Jin ¹, Pohlee Cheah ² , Jing Qu ², Lijuan Liu ¹ and Yongfeng Zhao ^{2,*}

¹ Department of Radiology, The Affiliated Tumor Hospital of Guangxi Medical University, Hedi Road No.71, Nanning 530021, China; jinguanqiao77@gxmu.edu.cn (G.J.); liulijuan@stu.gxmu.edu.cn (L.L.)

² Department of Chemistry, Physics and Atmospheric Science, Jackson State University, Jackson, MS 39217, USA; pohlee.cheah@jsums.edu (P.C.); jing.qu@students.jsums.edu (J.Q.)

* Correspondence: yongfeng.zhao@jsums.edu

Academic Editor: Clare Hoskins

Received: 8 September 2020; Accepted: 13 October 2020; Published: 16 October 2020



Abstract: Melanoma is an aggressive form of skin cancer with a very high mortality rate. Early diagnosis of the disease, the utilization of more potent pharmacological agents, and more effective drug delivery systems are essential to achieve an optimal treatment plan. The applications of nanotechnology to improve therapeutic efficacy and early diagnosis for melanoma treatment have received great interest among researchers and clinicians. In this review, we summarize the recent progress of utilizing various nanomaterials for theranostics of melanoma. The key importance of using nanomaterials for theranostics of melanoma is to improve efficacy and reduce side effects, ensuring safe implementation in clinical use. As opposed to conventional in vitro diagnostic methods, in vivo medical imaging technologies have the advantages of being a type of non-invasive, real-time monitoring. Several common nanoparticles, including ultrasmall superparamagnetic iron oxide nanoparticles, silica nanoparticles, and carbon-based nanoparticles, have been applied to deliver chemotherapeutic agents for the theranostics of melanoma. The application of nanomaterials for theranostics in molecular imaging (MRI, PET, US, OI, etc.) plays an important role in targeting drug delivery of melanoma, by monitoring the distribution site of the molecular imaging probe and the therapeutic drug in the body in real-time. Hence, it is worthwhile to anticipate the approval of these nanomaterials for theranostics in molecular imaging by the US Food and Drug Administration in clinical trials.

Keywords: theranostics; nanomaterials; melanoma; molecular imaging

1. Introduction

Malignant melanoma (MM) is one of the deadliest skin cancers that may occur in any anatomical site of melanocytes. There were 351,880 newly diagnosed cases of malignant melanoma worldwide in 2015, which accounts for 80% mortality of skin cancer [1]. Especially, the five-year survival rate of metastatic melanoma is only 10%, and the median survival period is less than 10 months [2]. Due to the invasiveness and metastasis ability of malignant melanoma, traditional chemoradiotherapy has a poor outcome. Hence, global melanoma experts have been exploring more effective treatment methods, constantly breaking through the limitations of traditional treatment, as well as overcoming the drug resistance [3].

Researchers are extensively searching for safe and effective single or combination treatments in vitro and in vivo, and further tested in clinical patients. These regimes are based on surgical treatment, adjuvant therapy, immunotherapy, targeted treatment, radiation therapy, and cancer-related immune checkpoints. With the recent development of clinical trials for triple therapy (combined BRAF/MEK inhibition with PD-1 blockade) and drug tolerance to target therapy analyzed at single cell

level in melanoma, we expect that the combination of treatments can not only enhance treatment efficacy but also prevent the emergence of drug resistance. Among these new diagnostic and therapeutic technologies, the integration of imaging and treatment technology has received great attention recently. This technology combines multi-modal imaging technology and treatment methods including photothermal therapy (PTT) [4], photodynamic therapy (PDT) [5], immunotherapy [6], and other new treatment methods [7]. These studies have shown very promising results in reducing the side effects of chemotherapy. In addition, the nano-drug delivery systems are able to target and release at the tumor site, reducing toxic side effects. The unique advantages of targeted nanocarriers loaded with drugs and imaging properties can greatly improve the effectiveness and specificity of therapy which is difficult to treat. This review is focused on the recent progress on the treatments of malignant melanoma by theranostic nanoparticles.

2. Melanoma

2.1. Introduction of Melanoma

The incidence of melanoma has been increasing rapidly over the years and accounts for 1–2% of all malignant tumors [8]. Melanoma originates from the outer ectoderm and about 60% of melanoma is caused by pigmentation. Over 90% of the primary lesions were found in the skin, and some were on the scalp, neck, palms, calves, soles, fingers (toes), etc. [9]. A few occurred in parts other than the skin, such as the eyes, esophagus, rectum, anus, and vagina. Melanoma is more common among middle-aged and elderly people, while patients under the age of 20 years old are rare [10]. This shows the prevalence of melanoma increases with age.

Risk factors for melanoma include heredity, sun exposure, trauma, and age [3,11,12]. Most melanoma mutations are part of the mitogen-activated protein kinase and phosphoinositol kinase pathway (MPK) [13]. Surgical treatment is essentially used for various subtypes of melanoma to remove the primary tumor [14]. In general, radiation therapy is not required after surgical resection of primary tumors, but radiotherapy is beneficial for some subtypes, such as desmoplastic neurotrophic melanoma (DNM), which could alleviate the local symptoms [15]. There are some adjuvant systemic therapies, such as cytotoxic drugs and immunotherapy. Common cytotoxic drugs for melanoma treatment include dacarbazine [16], temozolomide [17], paclitaxel [18], and carboplatin [19].

Due to the strong immunogenicity of melanoma tumors, immunotherapy has always played an important role in the treatment of melanoma. The immunological checkpoint inhibitors for melanoma are comprised of monoclonal antibodies targeting cytotoxic T lymphocyte-associated antigen 4 (CTLA-4) and apoptosis-1 protein (PD-1). The current clinical application of ipilimumab against the immune checkpoint receptor CTLA-4 has shown to significantly improve progression-free survival (PFS) and overall survival (OS) in patients with unresectable melanoma [20]. Currently, anti-PD-1 antibodies mainly consist of nivolumab and pembrolizumab [21]. Pembrolizumab is a highly selective human-derived anti-PD-1 monoclonal antibody that inhibits PD-1 receptors. Pembrolizumab is the world's first FDA-approved antibody that targets PD-1 in the treatment of advanced melanoma.

Small molecule targeted therapy has been developed for melanoma with genetic variants such as BRAF, NRAS, and c-KIT. In addition, antagonistic drugs for targeting each gene mutation have begun to be used in clinical treatment [22,23]. Most BRAF mutations that occur in melanoma are located at the V600 stump, usually V600E, sometimes V600K or the others [24]. The BRAF inhibitors have clinical therapeutic effects on melanoma with BRAFV600 mutation. MEK acts as a downstream molecule of BRAF, in which the MEK inhibitors can further enhance the therapeutic effect. The c-KIT mutations are often associated with mucosal and acromegaly melanoma. Imatinib is a c-KIT mutation inhibitor, and phase II clinical trial data have demonstrated that the imatinib treatment of c-KIT mutations or c-KIT-expanded metastatic melanoma will give an overall response rate of 20–30%, disease control rate of 35–55%, but most of the relief duration is limited [25]. The use of interferon-alpha (IFN- α), especially in high doses for the treatment of melanoma patients having a high risk of recurrence,

has been widely exercised in the clinical practice [26]. High doses of interleukin-2 (IL-2) have been used as first-line and second-line treatment of metastatic melanoma [27]. Local injection of these drugs is confirmed to have the therapeutic effect in a number of clinical trials, but more as a second-line treatment. Local treatments include talimogene Laherpaprepvec (T-VEC), intralesional injection of BCG, interferon, IL-2, local ablation. Topical imiquimod was reported for superficial skin lesions treatment [28–30].

Imaging examinations including chest, abdomen, pelvic enhanced X-ray computed tomography (CT), whole-body positron emission tomography-CT (PET-CT), head magnetic resonance imaging (MRI) were commonly used to provide information at different stages of disease management [31,32]. The CT scan showed that the tumor mass has a slightly lower density and moderate enhancement. For patients with stage IIIc or stage IV melanoma, head MRI should be considered. MRI scans created strong paramagnetism in melanoma tissues. The MM lesion will show short T_1 and short T_2 signals on MRI. Therefore, MRI is the best imaging diagnosis method for intracranial melanoma. The PET-CT examinations were used to help detect occult metastatic lesions [33]. Generally, melanoma at stage 0, IA, and IB do not require routine imaging examination. When a specific sign or symptom suggests a possible metastatic melanoma, an imaging examination is recommended regardless of the patient's stage. For stage I/II patients, the physical examination on highly suspected regional lymph node metastasis should be conducted before the sentinel lymph node biopsy. In particular, the lymph node ultrasonography cannot be a replacement for sentinel lymph node biopsy [34]. Moreover, for clinical suspicious lymph nodes, a biopsy is performed even if the ultrasound finding is negative. Patients in stage III and IV undergo the corresponding imaging examinations to assess the extent of lesions and baseline status.

2.2. Melanoma Animal Model

The earliest melanoma animal model was established using freshwater swordtail fish in the central United States. However, the application is limited due to the evolutionary gap between the swordtail fish system and mammals, and the discrepancies of its tumors from human melanoma [35]. Since then, South American possums have also been reported as melanoma models [36]. However, the genetic traits of this animal were not defined, and the possum does not produce malignant melanoma, unlike human melanoma. Current applications of nanotechnology for melanoma imaging and treatment are focused on the preclinical stage and studies using animal models for in vivo studies [37,38]. Syngeneic mouse model is commonly used as the animal model closely mimics human metastatic melanoma. Some melanoma cell lines were used, such as A375, B16F10, SK-Mel28 human melanoma cells, and SK-MEL-37 melanoma cell line. B16-F0, -F1, -F10, and -BL6 mouse melanoma cell lines are used to model the human metastasis process due to the ability of these cells to metastasize from the primary site into different organ tissues. With regard to the characteristic difference among B16 melanoma cell lines, Taniguchi et al. [39] reported that the decrease in the expression of β m actin, acidic actin coexpressed with β , γ -actins, was associated with high risk in invasiveness and metastasis in several B16-melanoma cell lines besides B16-F1 and B16-F10. Sadano H et al. [40] demonstrated that B16-F10 cells transfected with expression plasmids of β m showed a decrease in invasive activity. Similarly, B16-BL6 cells transfected with β m decreased in the in vivo invasiveness, i.e., metastasis in the lung and the in vitro invasion of collagen gels, as well as the cell migration after treated with colloidal gold particles [41]. Sadano H et al. [42] indicated that B16-F1 cells have a higher expression of vinculin, a membrane-associated cytoskeletal protein, than in B16-F10 cells. The transplantation site and methods of melanoma mouse xenograft model mainly include intraperitoneal injection, intraocular injection, tail vein injection, and subcutaneous tissue injection [43]. Intraperitoneal injection study is inconvenient for the dynamic detection of tumor growth [44]. A tail vein injection is used to establish the metastatic tumor model of melanoma, however, it is the most difficult operation among others. Subcutaneous tissue injection is the simplest and most obvious way to observe the tumor. The inoculation sites including subcutaneous skin, subcutaneous foot, and others are selected as needed.

3. Molecular Imaging

3.1. General Aspects

The advancement of biomedical imaging tools has provided benefits for the diagnosis of various diseases. Images obtained through different imaging techniques can provide crucial information because of enhanced signals in the lesion. Similarly, the diagnosis of melanoma is mainly identified based on the comparison with the signals from the surrounding normal tissues. The application of theranostic nanomaterials in melanoma is mainly focused on using multi-modality imaging techniques to achieve early diagnosis of a disease and provide the needed treatment plan (Figure 1a–c) [45–47]. Advanced medical imaging technologies include optical imaging, ultrasonic imaging (US), X-ray computed tomography (CT) imaging, magnetic resonance imaging (MRI), single-photon emission computed tomography (SPECT) imaging, and positron emission tomography (PET) imaging.

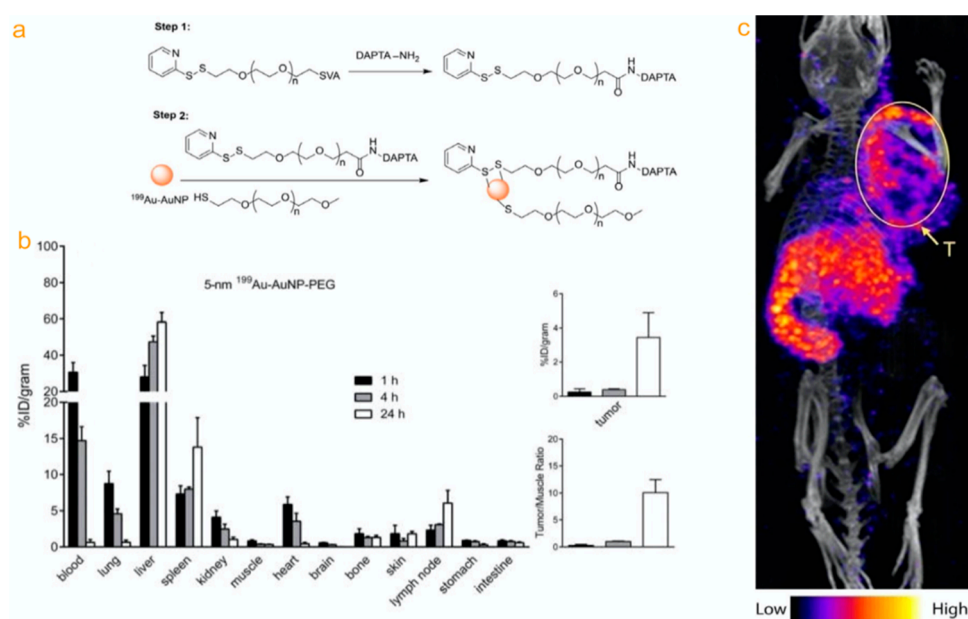


Figure 1. (a) ¹⁹⁹Au-AuNP-DAPTA for SPECT in the context of cancer diagnosis. Schematic illustration has shown the synthesis of ¹⁹⁹Au-AuNP-DAPTA. (b) Biodistributions of the 5nm ¹⁹⁹Au-doped AuNPs in 4T1 tumor-bearing mice. (c) Nano SPECT/CT image of a 4T1 tumor-bearing mouse injection of the 5-nm ¹⁹⁹Au-AuNP-DAPTA probe. Reproduced from [47] with permission.

Compared with in vitro diagnostic methods, medical imaging technology has the advantages of being non-invasive, real-time monitoring, and being more accurate. However, each imaging method differs in the sensitivity, penetration, resolution, detection limit, analysis time, and safety concern. CT imaging provides great resolution for tissues with different density but has radiation hazards. US is cheaper and widely used in the clinic but required a highly skilled and experienced operator. PET and SPECT are more sensitive imaging methods, with deeper tissue penetration. However, they have a lower spatial resolution of imaging and carry the potential risk of radiation exposure. Fluorescence imaging is highly safe and sensitive, enabling fast, dynamic, real-time monitoring, but is difficult to do accurate quantitative analysis in vivo. MRI has strong tissue penetrability, it is non-invasive, with no radiation hazard, high spatial resolution, and it directly or indirectly displays more abundant structural information in living organisms. However, the biggest limitation of MRI imaging is that the imaging is easily affected by motion and metal. At present, medical imaging is used to study cells, tissues, and organisms through changes in specific molecules, proteins, and genes in melanoma biological processes, which plays an important role in the clinical diagnosis and treatment of melanoma [48–50].

3.2. Molecular Imaging for Diagnosis

3.2.1. Magnetic Resonance Imaging (MRI)

MRI is a non-invasive diagnostic test that uses a high magnetic field and radiowaves to construct images of the human body without harming the normal tissue cells. MRI can obtain tomographic images in all directions, for example, 3D volume images. The combination of nanomaterial and MRI technology can further improve the sensitivity and accuracy of the test. Therefore, magnetic nanomaterials are the most widely studied. Ultrasmall superparamagnetic iron oxide nanoparticles (USPIONs) have gained interest among the researchers for intracellular drug delivery application. However, the study on the cellular reactions and mechanisms upon nanoparticles uptake is not well illuminated. Cengelli F et al. [51] demonstrated that AminoUSPIONs were internalized by human melanoma cells via clathrin-mediated uptake in the lysosomes, then activating the lysosomal cathepsin D and reducing the expression of the transferrin receptor. This result showed that AminoUSPIONs could invade tumors and induce melanoma cell response. Pintaske, J. et al. [52] studied the effect of magnetically labeled cells in vitro and reported the cellular transverse relaxation at the spin-echo sequence increases with the magnetic field. The cellular transverse relaxivities at the gradient-echo sequence were slightly higher under the same magnetic field. Sundstrom T et al. [53] indicated no changes in cell activities and viabilities upon SPION exposure across several in vitro assays. MRI for SPION-labeled melanoma cells after injection into the left cardiac ventricle of mice showed no changes in apoptosis. Several SPION-labeled cell lines also displayed similar results in cerebral imaging and in vivo histology studies. The metastasis process resembling human cancers was unaffected by SPION labeling.

Based on the above studies, superparamagnetic iron oxide nanoparticles could become the carrier of targeted drug delivery. Vannucci L et al. [54] investigated the in vivo melanoma-targeting ability of human protein ferritin (HFt)-based nanovector (HFt-MSH-PEG), functionalized with α -melanocyte-stimulating hormone (α -MSH) and stabilized by poly(ethylene glycol) (PEG) molecules. HFt-MSH-PEG NPs exhibited very high selectivity, accumulating and targeting at the primary melanoma as compared to the control HFt-PEG NPs with no α -MSH moiety. These results indicated that HFt-MSH-PEG NPs can be used as promising carriers to deliver diagnostic or therapeutic agents to cutaneous melanoma sites selectively in vivo. Hundt W et al. [55] evaluated the M21 and M21-L tumors with a size of 850 mm³ by intravenously treatment with an $\alpha(v)\beta(3)$ -integrin-ligand-coupled nanoparticle (RGDNP)/RAF(-) complex for five times every three days. MRI scans at a set time interval of 24 h and 72 h showed a significant reduction in the contrast uptake and an increase in the diffusion coefficient of the tumors after the targeted gene delivery therapy. Schmieder AH et al. [56] determined that $\alpha(v)\beta(3)$ -targeted paramagnetic nanoparticles can be used to study the development of nascent melanoma xenografts in an athymic nude mice model by tracking the sparse $\alpha(v)\beta(3)$ integrin expression on neovasculature. Contrast enhancement in the neovascularity of the animals that accumulated with $\alpha(v)\beta(3)$ -targeted paramagnetic nanoparticles increased by 173% after 120 min at 1.5T. Meanwhile, non-targeted paramagnetic nanoparticles had a 50% lower signal contrast than that in the targeted group. MRI results were further corroborated by the histology study. To confirm the bioactivity of the targeted nanoparticles, a competitive cell adhesion assay was performed. The incubation of $\alpha(v)\beta(3)$ -expressing cells with targeted nanoparticles significantly inhibited the binding of the cells to a vitronectin-coated surface. Boles KS et al. [57] utilized MRI to compare the 3-dimensional spatial distribution of Robo4 and $\alpha(v)\beta(3)$ -integrin as the biosignatures of angiogenesis in a rapidly growing tumor. The results suggested that $\alpha(v)\beta(3)$ -integrin and Robo4 are important biomarkers in syngeneic mouse tumors for noninvasive MR molecular imaging.

3.2.2. Single-Photon Emission Computed Tomography (SPECT)

Single-Photon Emission Computed Tomography (SPECT) imaging has advantages such as high sensitivity, quantitative analysis, combined therapy, no tissue depth limitation, systemic imaging, and monitoring biochemical changes in vivo. In recent years, extensive research has been dedicated to developing SPECT contrast agents with high specificity and affinity. Early detection of tumor tissue and intracellular metabolic changes can be achieved prior to their morphological changes by using specific molecular probes that link to these tracers. Baishya, R. et al. [58] fabricated PLGA nanoparticles loaded with ursolic acid (UA) (UA-NPs) as the drug carrier and compared the tumor-targeting effects of free UA and UA-NPs in B16F10 melanoma cells in vitro and in vivo. The study on tumor targeting potential of UA-NPs in B16F10 melanoma cell lines gave a promising result. Portilho, F.L. et al. [59] studied a new in vivo drug delivery system using mesoporous silica nanoparticle with a magnetic core. The results demonstrated the great efficiency to dope the nanoparticle with dacarbazine (>98%), as well as labeling with ^{99m}Tc (>99%). The in vivo study on mice model with melanoma demonstrated the increased permeability and retention effect of the magnetic core-mesoporous silica nanoparticles when injected intratumorally. These nanoparticles proved to be a reliable and efficient contrast agent for melanoma. Allen, K.J.H. et al. [60] demonstrated that a humanized antibody that targets “free” melanin in the tumor microenvironment had highly accumulated in B16F10 murine melanoma in C57Bl/6 mice through microSPECT/CT scan. The results demonstrated that the h8C3 antibody labeled with ^{213}Bi is a potential reagent to treat metastatic melanoma patients in the clinical trial.

3.2.3. Optical Imaging

Optical imaging usually uses two techniques: bioluminescence imaging (BLI) and fluorescence imaging (FI). The former employs a luciferase gene (such as FLUC, RLUC, and GLUC) to label cells or DNA, in which its expression product reacts with a firefly substrate to produce fluorescence. The latter uses a variety of fluorescent protein genes (such as GFP, RFP, YFP, etc.), organic fluorescent dyes, fluorescent up-converting nanoparticles, quantum dots. Optical molecular imaging technology can directly detect metabolic dynamic processes in vivo, protein and protease activities, and gene behavior, which is helpful in the monitoring of specific molecules and gene expression. However, the in vivo application of optical imaging is limited due to the instability and potential toxicity of fluorescent molecules, the scattering of light in the body, and the superficial depth of detection. McCormack, D.R. et al. [61] conjugated melanoma cells with gold nanoparticles to enhance the sensitivity in a photoacoustic detection system. AuNP-tagged melanoma showed an overall signal increase of 34% higher than the untagged cells (Figure 2a–d). There is a maximum signal difference of 0.295 mV/mJ at 500 nm, an increase of 41%. Shields, C.L. et al. [62] investigated whether an infrared dye-conjugated virus-like nanoparticle (AU-011) could be used to treat small choroidal melanoma by inducing tumor regression and minimizing the vision loss. This novel nanoparticle therapy is currently under clinical trial as a potential alternative to conventional plaque radiotherapy treatment which offered tumor control but may potentially lead to vision loss. Chen, F. et al. [63] applied ultrasmall fluorescent (Cy5) silica nanoparticles (C' dots) for melanoma-selective imaging. PEG-Cy5-C' dot nanoparticles were conjugated with αMSH peptide sequences and targeted melanoma in xenografted melanoma mouse models. The results demonstrated a nearly 10-fold improvement in MC1-R affinity for nanoparticles attached with αMSH peptide as compared to using native peptide alone. These findings promise the clinical translation of αMSH -PEG-Cy5-C' dots as the peptide and antibody-based probes for image-guided surgery and therapy.

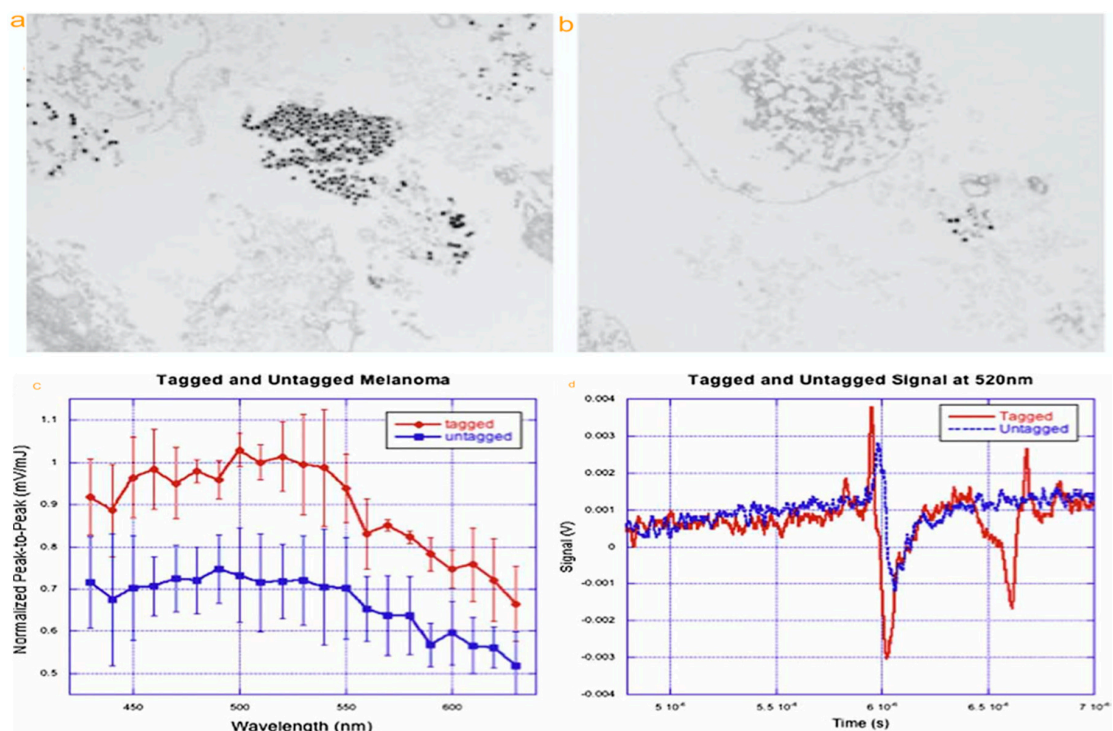


Figure 2. TEM images of tagged (a) nanoparticle and untagged melanoma cells (b). Two pictures have demonstrated tagged cell (c) significantly increased signal but minimally increased in photoacoustic signal (d) compared with untagged melanoma. Reproduced from [61] with permission.

3.2.4. Photoacoustic Imaging

Photoacoustic imaging can be effectively used to perform biological tissue structure and functional imaging and provide an important method for studying biological tissues. It is especially useful for early detection and treatment monitoring of cancer. Li, X. et al. [64] successfully prepared a polymeric multifunctional nanoparticle probe targeting melanoma in photoacoustic/ultrasound dual-mode imaging. The probe is constructed by gold nanorods (Au-NRs) and liquid perfluorocarbon (perfluorinated hexane/PFH), then attached with a monoclonal antibody (MAGE-1 antibody) which targets melanoma-associated antigens (MAGE) (MAGE-Au-PFH-NPs) (Figure 3a–c). Cell-targeting experiments illustrate large numbers of MAGE-Au-PFH-NPs surrounding B16 melanoma cells. The photoacoustic signal was enhanced with increased Au-NR concentration after laser irradiation at 808 nm. A cytotoxicity study showed that MAGE-Au-PFH-NPs have good biocompatibility. This confirms that MAGE-Au-PFH-NPs can be employed as a photoacoustic/ultrasound dual-modality contrast agent that offers noninvasive monitoring and treatment of tumors.

3.2.5. Positron Emission Tomography (PET)

The main substance used in PET imaging is fluorodeoxyglucose, which is a substance required for biological life metabolism and is accumulated in high-metabolism tumor tissues at different metabolic states. On the other hand, less fluorodeoxyglucose is accumulating in normal tissues with low metabolism, as reflected in the PET images. In recent years, radioisotope-labeled metallic materials have been found to have potential use in PET imaging. Chen, F. et al. [65] introduced a multifunctional nanoparticle platform with radioiodinated (^{124}I , $t_{1/2} = 100.2$ h) on cRGDY-conjugated fluorescent silica nanoparticles (C dots). The pharmacokinetic profiles showed high tumor-targeting efficiency. The ^{89}Zr -labeled (^{89}Zr , $t_{1/2} = 78.4$ h) ultrasmall hybrid organic-inorganic particle featured excellent radiobiological properties as a suitable PET tracer for enhanced molecularly targeted cancer imaging applications in clinical use. Zhao, Y. et al. [45] synthesized gold nanocages (AuNCs) attached with

α -melanocyte-stimulating hormone (α -MSH) peptide and radiolabeled with ^{64}Cu for melanocortin 1 receptor-(MC1R) targeted PET. AuNCs have a well-defined structure and high radiolabeling efficiency. The results indicated the potential use of targeted AuNCs for melanoma theranostics (Figure 4a,b).

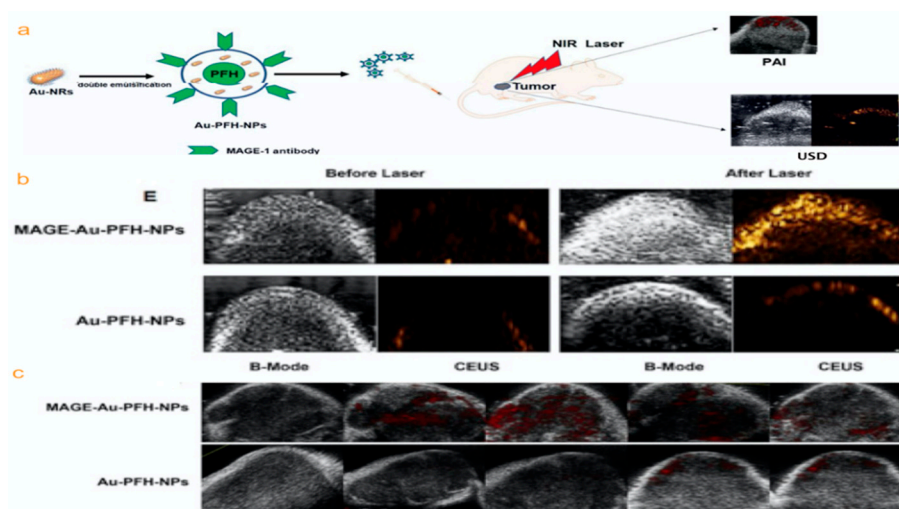


Figure 3. Schematic illustration of the MAGE-Au-PFH-NPs synthesis strategy and as-synthesized NP imaging (a). B16 tumor-bearing nude mice before vs after treatment (b), and different time point treatment between Au-PFH-NPs and MAGE-Au-PFH-NPs (c). Reproduced from [64] with permission.

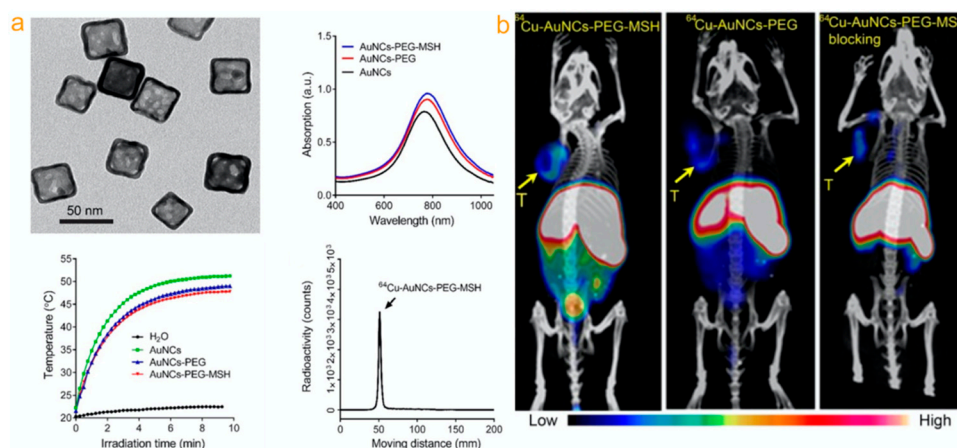


Figure 4. Melanocortin 1 receptor targeted PET/CT imaging of melanoma with gold nanocages. Characterization of gold nanocages (a). PET/CT images of mice-bearing B16/F10 melanoma intravenously injected with ^{64}Cu -AuNCs-PEG-MSH through tail vein had detected tumor uptake in different times (b). Reproduced from [45] with permission.

4. Molecular Imaging for Theranostics

Most of the research on nanomaterials as drug carriers is mainly dedicated to increasing the concentration of drugs carried to the tumor tissues and reducing the exposure of normal tissues by means of their active targeting. When it comes to drug delivery, the ability to monitor drug delivery and release will significantly improve treatment by adjusting the dosage and frequency based on the real-time drug uptake information. Imaging guided therapy (theranostics) is a therapeutic method where targeting localization and drug delivery are guided and monitored through noninvasive imaging. Theranostic strategy could assist in making a personalized treatment plan, as well as helping to evaluate a patient's response to treatment. In regard to increase drug concentration and to achieve accurate and efficient treatment, magnetically targeted drug delivery has received a lot of attention. The principle of

using SPION for drug delivery application is to combine the drug into SPION by chemical bonding or physical interaction to form a complete drug delivery system. This system can guide the drug to the target site via an external magnetic field force and is released at a fixed point to increase the drug concentration at the target region and reduced the side effects of the drug. Balivada, S. et al. [66] successfully designed bi-magnetic Fe/Fe₃O₄ core/shell nanoparticles and checked its effectiveness for cancer targeting via intratumoral or intravenous administration. The 4-tetracarboxyphenyl porphyrin (TCPP) units were conjugated to offer photosensitive activity. After intratumoral injection, the magnetic hyperthermia results implied that micromolar concentrations of iron caused a significant anti-tumor effect on murine B16-F10 melanoma under three short 10-min alternating magnetic field (AMF) exposures. Results showed that the tumor size decreased after intravenous administration of the MNPs and exposure to AMF a day after the injection for three consecutive days.

Zhao, J. et al. [67] have synthesized the anti-tumor potential of macrophages, harnessed by ferumoxytol (FMT), combined with the Toll-like receptor 3 (TLR3) agonist, poly (I:C) (PIC), and FP-NPs (nanoparticles composed of amino-modified FMT (FMT-NH₂) and surface functionalized with PIC). The ferumoxytol (FMT) synergized with the Toll-like receptor 3 (TLR3) agonist poly (I:C) (PIC), prompting the macrophage activation for primary and metastatic melanoma regression.

Researchers have developed a variety of fluorescent contrast agents with a range of excitation/emission wavelengths using fluorescent molecules or nanoparticles. However, organic fluorescent dyes are often subjected to their relatively poor photostability, which is not conducive to long-term fluorescence monitoring of pathological changes in tumor tissues. Improving the light stability of organic fluorescent dyes is one of the active areas of current studies. In addition, red shifting the excitation and emission of organic fluorescent dyes to the infrared region is also beneficial for biomedical applications. This is due to the better tissue penetration properties of infrared light comparing to ultraviolet and visible light, extending the application of organic fluorescent dyes in deep biological tissues. Moreover, the development of organic fluorescent dyes with biological active small molecules, capable of monitoring dynamic physiological reactions in biological tissues, is of great significance for the integration of diagnosis and treatment of cancer.

Tang, J. et al. [68] synthesized a carboxylated poly (amido-amine) (PAMAM) loaded with chemotherapeutic drugs, temozolomide (TMZ), and fluorescent dye indocyanine green (ICG) and used as drug delivery nanocarrier. Moreover, the surface of nanocarrier was conjugated with hyaluronic acid (HA), which targets the CD44-overexpressing cancer cells to enhance its selectivity to kill melanoma cells. The ICG-encapsulated nanoparticles also demonstrate a good capability to produce heat and singlet oxygen under near-infrared (NIR) light (808 nm) irradiation. In vivo imaging measurement demonstrated that the ICG-loaded nanoparticle was actively targeting the tumor site. In vitro and in vivo experiments confirmed the synergistic effect of having both TMZ and ICG loaded on the nanoparticle to effectively kill melanoma cells and inhibit their growth after NIR light irradiation.

Tchounwou, C. et al. [69] developed a hybrid theranostic platform by attaching anti-GD2 antibody to gold nanoparticle (GNP), conjugated with single-wall carbon nanotube (SWCNT) for photothermal therapy. Due to strong plasmon coupling, modified GNP has six orders of magnitude higher luminescence signal than those from unmodified GNP or SWCNT alone.

Ultrasound microbubbles as a drug carrier for disease treatment have the following advantages: Ultrasonic microbubbles produce cavitation effects under lower sound pressure, which can cause adjacent endothelial cells to produce instantaneous repairable tiny pores or increase the gap between endothelial cells. Drugs released in the blood or microbubbles can enter the cell or smoothly pass through the blood vessels, thereby increasing the cellular uptake of the drug. Ultrasonic microbubbles carrying the drugs to the cells can better reserve the activity of the drug when the microbubbles are being crushed at a higher sound pressure to release the drugs, and therefore achieve the purpose of ultrasonic controlled drug release. For the effects of acoustic microfluidics, sonochemistry, shock waves, and liquid microjets, they can increase the transmission of drugs to target cells.

Harada, Y. et al. [70] investigated the effect of US irradiation on melanoma cell (C32) in the presence or absence of titanium dioxide (TiO₂) nanoparticle. Cell viability was tested immediately after US irradiation. Meanwhile, the tumor volume regression was measured on subcutaneously implanted C32 solid tumors in mice under US exposure (1MHz, 1.0 W/cm², 2 min duration). The cell viability was significantly reduced only after US irradiation combined with TiO₂. In vivo results showed the significant suppression of tumor growth with the complementary treatment with TiO₂ and US exposure. Both in vitro and in vivo results have demonstrated the effectiveness of killing melanoma cells using TiO₂ nanoparticles under the irradiation of US.

5. Outlook

Before the approval of ipilimumab in 2011, dacarbazine had become the standard chemotherapeutic agent for the treatment of melanoma. Temozolomide is often a substitute for an oral equivalent of dacarbazine in the case of central nervous system involvement because temozolomide can cross the blood-brain barrier. Although chemotherapy does not confirm overall survival benefit, chemotherapy provides patients with palliative treatment options. The 5-year survival rate is usually 5–10% for patients with advanced malignant melanoma using standard chemotherapy [71]. For a large proportion of patients with advanced melanoma, the approval of checkpoint inhibitors is an important milestone to increase long-term survival. Targeted therapy and immunotherapy are now available as approved first- and second-line therapies for patients with BRAFV600 mutations [72]. It is important to determine which regime of these therapies (chemotherapy, targeted therapy, and immunotherapy) is most effective. Long-term follow-up and a full assessment of the benefits of PD-1 blockade for patients with melanoma are required. Although the incidence of PD-1 inhibitors toxicity is very low, the immune-related adverse events can still be severe or even fatal in rare cases [73]. There are still a significant number of patients exhibiting innate resistance or resistance to any approved immunotherapy. So, new treatment options or combinations are needed for these patients with melanoma.

Nanotechnology has many superior properties, making it more and more widely used in the field of melanoma diagnosis and treatment, bringing new ideas to solve the problems in traditional melanoma diagnosis and treatment. Drug delivery for targeted therapy of melanoma by nanoparticles has included the delivery of chemotherapeutics, siRNA, monoclonal antibody, shRNA, dDNA, vaccination, immunotherapy, photothermal treatment, and multi-drug (multifunctional particles, multi-mode particles, chemo-thermo-immuno therapy), but it has remained challenging. So far, many studies have used nanotechnology to overcome drug resistance. Tran, M.A. et al. [74] have shown that nanoliposomal ceramide enhances the effectiveness of sorafenib by causing synergistic inhibition, as well as preventing drug resistance. Pegoraro, C. et al. [75] encapsulated doxorubicin in polymersomes which exhibited selectivity to melanoma cells, compared with healthy fibroblasts. Doxorubicin conjugated with PEG-lipids enhanced the cellular uptake of doxorubicin and promoted cellular retention by two-fold. This could help to greatly improve drug efficacy and prevent the efflux protein activity in multidrug-resistant cancer cells. Results have demonstrated the ability of the targeted liposomal to treat and overcome doxorubicin resistance in cancer cells.

Currently, most NPs are evaluated as drug delivery carriers in standard two-dimensional (2D) cell cultures in vitro. However, in vitro cell cultures often fall short of the tumor microenvironment in vivo. Thus, most studies on NP efficacy in 2D cultures often lack predictability, while animal models are costly and bring about ethical dilemmas. In vitro 3D melanoma models will be established to better evaluate the therapeutic effects of NPs. A single NP agent with multi imaging modalities is desired for non-invasive imaging in clinical translation [76].

Multi-modality imaging probes offer the solution to multiple issues, such as the resolution, sensitivity, and tissue penetration. By overcoming the limitations of each imaging modality, the multimodality technology has complementary and cross-validation capabilities. In addition to a simple multi-function NP-combined imaging function, image-guided drug delivery not only improves the tumor nanotheranostics but also monitors the treatment outcomes and assists in optimizing the

nanotheranostics regimens (Figure 5a–c) [77]. However, the mechanisms of melanoma resistance have been shown to be diverse [78]. Depending on the mechanism of the acquired drug resistance, different drugs will need to be used in the nanoparticles. It is undeniable that nanomaterials are still in the initial stage of cancer diagnosis and treatment, and a large number of animal experimental data and clinical trial evaluations are necessary before truly transforming into clinical practice. In the future, nanomaterials will not be used just for the diagnosis or treatment of tumors but will tend to be a tool for multifunctional diagnosis and treatment of tumors.

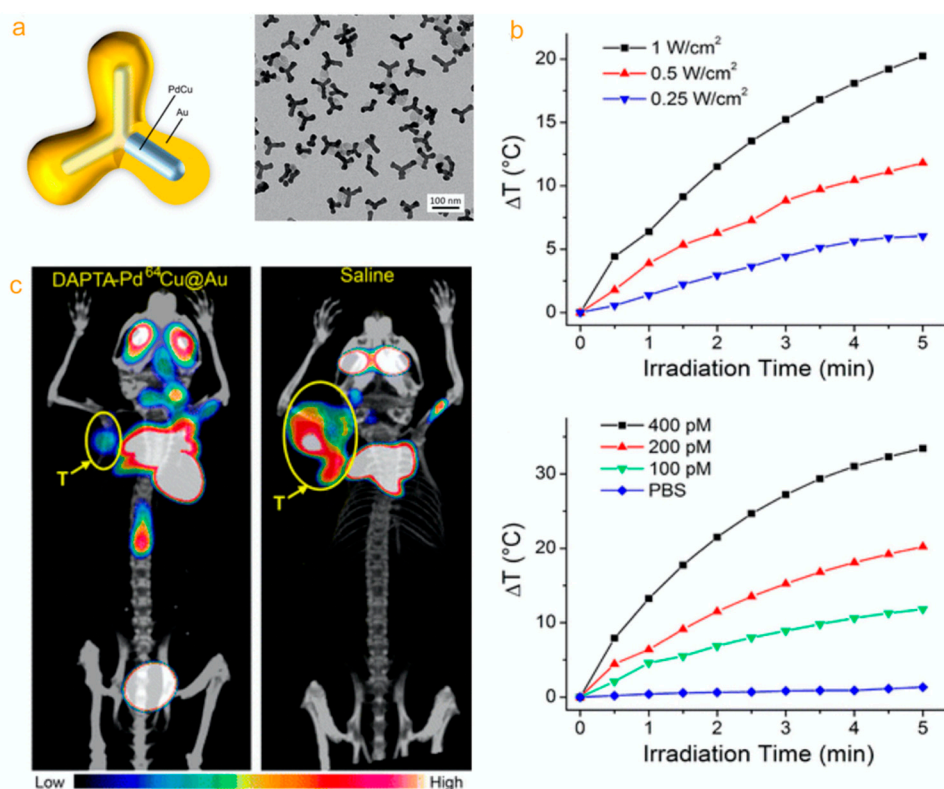


Figure 5. (a) ⁶⁴Cu-doped PdCu@Au tripods. Synthesis and characterization of PdCu@Au core–shell tripods. (b) Biodistributions of the ⁶⁴Cu-doped nontargeted tripods in an orthotopic mouse. (c) ¹⁸F-FDG PET/CT images of mice intravenously injected with an aqueous suspension of ⁶⁴Cu-doped, CCR5-targeted tripods compared with saline through the tail vein. ⁶⁴Cu-doped PdCu@Au tripods were a multifunctional platform for positron emission tomography and image-guided photothermal cancer treatment. Reproduced from [77] with permission.

6. Conclusions

The application of nanomaterials in molecular imaging (MRI, PET, US, OI, etc.) plays a major role in targeting drug delivery of melanoma because the distribution site of the molecular imaging probe in the body is consistent with the distribution site of the therapeutic drug in the body. However, the main technical bottlenecks restricting its development need to be solved, such as the design and preparation of targeted molecular imaging probes with high efficiency, specificity, stability, penetrability, as well as extraction and analysis of functional molecular imaging signal correlate with the clinical disease (Figure 6a–c) [79–82]. The solution to these problems requires contributions from molecular biology, clinical medicine, mathematics (modeling and analysis), physics (imaging principle), chemistry (probe synthesis), nanotechnology, biomedical signal processing (detection and processing), and many other disciplines. On the other hand, the toxic effects of nanomaterials cannot be ignored as studies on the toxicity of nanomaterials are still inconclusive. At the cellular level, nanomaterials can affect normal cells through cytotoxicity [83], genotoxicity [84], or genetic regulation [85]. At the tissue level, different

nanomaterials have different metabolic modes [86]. Moreover, they will accumulate in specific tissues and organs to produce toxicity. With the continuous development of nanotechnology, nanomaterials with unique physicochemical properties and tunability can be specifically modified to become a class of medical materials with targeted anti-tumor capability [47]. Despite the challenges mentioned above, nanomaterials for theranostics in molecular imaging have shown great promise in treating melanoma. New nanomaterials for theranostics in molecular imaging may be designed to have a higher therapeutic loading capacity and a tunable payload releasing profile. Recently developed genome editing technology may also provide a great opportunity in nanomaterials for theranostics in molecular imaging for treating melanoma.

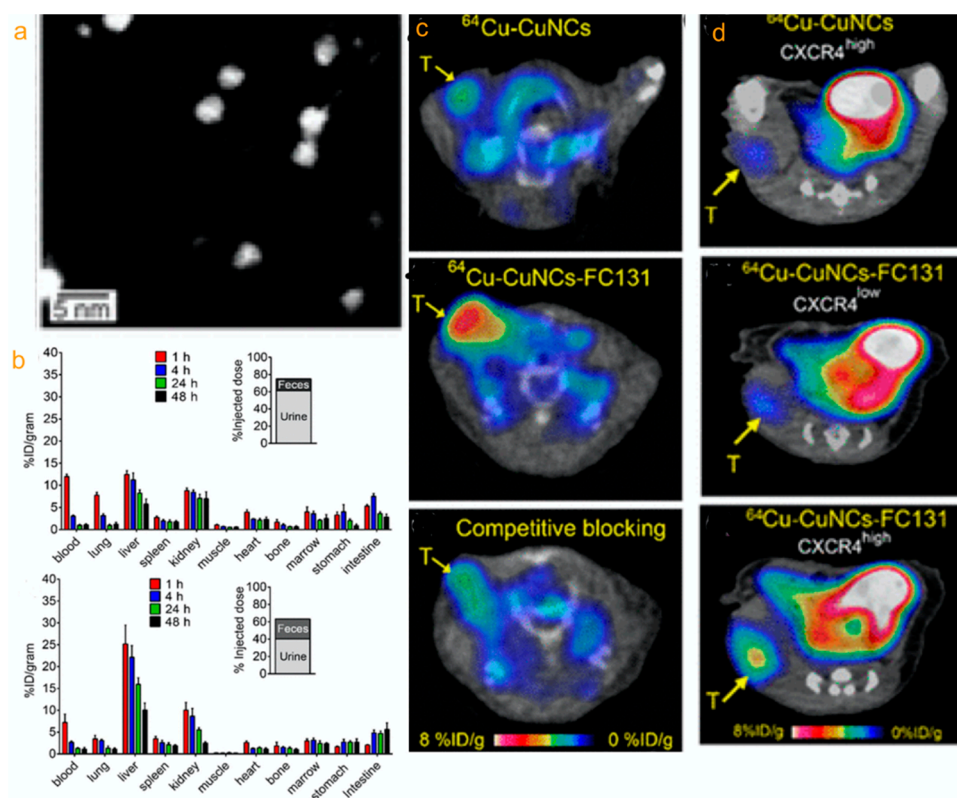


Figure 6. CXCR4-targeted ^{64}Cu -CuNCs for cancer theranostics. ^{64}Cu -CuNCs STEM (dark field) (a). Biodistribution and clearance of ^{64}Cu -CuNCs and ^{64}Cu -CuNCs-FC131 in female C57BL/6 mice. (b) In vivo PET imaging in female C57BL/6 mice injected ^{64}Cu -CuNCs and ^{64}Cu -CuNCs-FC131 at 24 h p.i. (c). In vivo PET imaging in a 4T1 mouse injected non-CXCR4-targeted ^{64}Cu -CuNCs and CXCR4-targeted ^{64}Cu -CuNCs (d). Reproduced from [82] with permission.

Funding: G.J. and L.L. were supported by Nature Science Foundation of China (grant number: 81260334 and 81760533).

Conflicts of Interest: The authors declare no conflict of interest.

References

1. Karimkhani, C.; Green, A.; Nijsten, T.; Weinstock, M.; Dellavalle, R.; Naghavi, M.; Fitzmaurice, C. The global burden of melanoma: Results from the Global Burden of Disease Study 2015. *Br. J. Dermatol.* **2017**, *177*, 134–140. [[CrossRef](#)]
2. Hodi, F.S.; O'Day, S.J.; McDermott, D.F.; Weber, R.W.; Sosman, J.A.; Haanen, J.B.; Gonzalez, R.; Robert, C.; Schadendorf, D.; Hassel, J.C.; et al. Improved Survival with Ipilimumab in Patients with Metastatic Melanoma. *N. Engl. J. Med.* **2010**, *363*, 711–723. [[CrossRef](#)]

3. Rastrelli, M.; Tropea, S.; Rossi, C.R.; Alaibac, M. Melanoma: Epidemiology, risk factors, pathogenesis, diagnosis and classification. *Vivo* **2014**, *28*, 1005–1011.
4. Wang, X.; Kang, C.; Pan, Y.; Jiang, R. Photothermal effects of NaYF₄:Yb,Er@PE3@Fe₃O₄ superparamagnetic nanoprobe in the treatment of melanoma. *Int. J. Nanomed.* **2019**, *14*, 4319–4331. [[CrossRef](#)] [[PubMed](#)]
5. Naidoo, C.; Kruger, C.A.; Abrahamse, H. Simultaneous Photodiagnosis and Photodynamic Treatment of Metastatic Melanoma. *Molecules* **2019**, *24*, 3153. [[CrossRef](#)] [[PubMed](#)]
6. Qian, J.M.; Yu, J.B.; Mahajan, A.; Goldberg, S.B.; Kluger, H.M.; Chiang, V.L. Frequent Use of Local Therapy Underscores Need for Multidisciplinary Care in the Management of Patients with Melanoma Brain Metastases Treated With PD-1 Inhibitors. *Int. J. Radiat. Oncol.* **2019**, *105*, 1113–1118. [[CrossRef](#)]
7. Bomar, L.; Senithilnathan, A.; Ahn, C. Systemic Therapies for Advanced Melanoma. *Dermatol. Clin.* **2019**, *37*, 409–423. [[CrossRef](#)]
8. Pavri, S.N.; Clune, J.; Ariyan, S.; Narayan, D. Malignant Melanoma: Beyond the Basics. *Plast. Reconstr. Surg.* **2016**, *138*, 330e–340e. [[CrossRef](#)]
9. Kibbi, N.; Kluger, H.; Choi, J.N. Melanoma: Clinical Presentations. *Cancer Treat. Res.* **2015**, *167*, 107–129. [[CrossRef](#)]
10. Hoejberg, L.; Gad, D.; Gyldenkerne, N.; Bastholt, L.; on behalf of the Academy of Geriatric Cancer Research (AgeCare). Trends in melanoma in the elderly in Denmark, 1980–2012. *Acta Oncol.* **2016**, *55*, 52–58. [[CrossRef](#)]
11. Berwick, M.; Buller, D.B.; Cust, A.E.; Gallagher, R.; Lee, T.K.; Meyskens, F.L.; Pandey, S.; Thomas, N.E.; Veierød, M.B.; Ward, S. Melanoma Epidemiology and Prevention. *Cancer Treat. Res.* **2015**, *167*, 17–49. [[CrossRef](#)]
12. Ossio, R.; Roldán-Marín, R.; Martínez-Said, H.; Adams, D.J.; Robles-Espinoza, C.D. Melanoma: A global perspective. *Nat. Rev. Cancer* **2017**, *17*, 393–394. [[CrossRef](#)] [[PubMed](#)]
13. Hayward, N.K.; Wilmott, J.S.; Waddell, N.; Johansson, P.; Field, M.A.; Nones, K.; Patch, A.-M.; Kakavand, H.; Alexandrov, L.B.; Burke, H.; et al. Whole-genome landscapes of major melanoma subtypes. *Nat. Cell Biol.* **2017**, *545*, 175–180. [[CrossRef](#)]
14. Koshenkov, V.P.; Broucek, J.; Kaufman, H.L. Surgical Management of Melanoma. *Cancer Treat. Res.* **2015**, *167*, 149–179. [[CrossRef](#)]
15. Thakar, S.; Kandl, T.; Sagiv, O.; Tripathy, D.; Tetzlaff, M.T.; Kapur, S.; Myers, J.; Hwu, W.-J.; Jaber, B.M.; Esmali, B. Desmoplastic Melanoma of the Periorbital Region. *Ophthalmic Plast. Reconstr. Surg.* **2018**, *34*, e48–e52. [[CrossRef](#)]
16. Hafeez, A.; Kazmi, I. Dacarbazine nanoparticle topical delivery system for the treatment of melanoma. *Sci. Rep.* **2017**, *7*, 16517. [[CrossRef](#)]
17. Li, R.-H.; Hou, X.; Yang, C.-S.; Liu, W.-L.; Tang, J.-Q.; Liu, Y.-Q.; Jiang, G. Temozolomide for Treating Malignant Melanoma. *J. Coll. Physicians Surg. Pak.* **2015**, *25*, 680–688.
18. Su, Y.; Hu, J.; Huang, Z.; Peng, B.; Xie, N.; Liu, H. Paclitaxel-loaded star-shaped copolymer nanoparticles for enhanced malignant melanoma chemotherapy against multidrug resistance. *Drug Des. Dev. Ther.* **2017**, *11*, 659–668. [[CrossRef](#)]
19. Chang, W.; Lee, S.J.; Park, S.; Choi, M.K.; Hong, J.Y.; Kim, Y.S.; Maeng, C.H.; Jung, H.A.; Kim, S.; Lee, J. Effect of paclitaxel/carboplatin salvage chemotherapy in noncutaneous versus cutaneous metastatic melanoma. *Melanoma Res.* **2013**, *23*, 147–151. [[CrossRef](#)]
20. Schadendorf, D.; Hodi, F.S.; Robert, C.; Weber, J.S.; Margolin, K.; Hamid, O.; Patt, D.; Chen, T.-T.; Berman, D.M.; Wolchok, J.D. Pooled Analysis of Long-Term Survival Data From Phase II and Phase III Trials of Ipilimumab in Unresectable or Metastatic Melanoma. *J. Clin. Oncol.* **2015**, *33*, 1889–1894. [[CrossRef](#)]
21. Ivashko, I.N.; Kolesar, J. Pembrolizumab and nivolumab: PD-1 inhibitors for advanced melanoma. *Am. J. Health Pharm.* **2016**, *73*, 193–201. [[CrossRef](#)] [[PubMed](#)]
22. Ponti, G.; Manfredini, M.; Greco, S.; Pellacani, G.; Depenni, R.; Tomasi, A.; Maccaferri, M.; Cascinu, S. BRAF, NRAS and C-KIT Advanced Melanoma: Clinico-pathological Features, Targeted-Therapy Strategies and Survival. *Anticancer. Res.* **2017**, *37*, 7043–7048. [[CrossRef](#)] [[PubMed](#)]
23. Sperduto, P.W.; Jiang, W.; Brown, P.D.; Braunstein, S.; Sneed, P.; Wattson, D.A.; Shih, H.A.; Bangdiwala, A.; Shanley, R.; Lockney, N.A.; et al. The Prognostic Value of BRAF, C-KIT, and NRAS Mutations in Melanoma Patients With Brain Metastases. *Int. J. Radiat. Oncol.* **2017**, *98*, 1069–1077. [[CrossRef](#)]

24. Hodis, E.; Watson, I.R.; Kryukov, G.V.; Arold, S.T.; Imielinski, M.; Theurillat, J.-P.; Nickerson, E.; Auclair, D.; Li, L.; Place, C.; et al. A Landscape of Driver Mutations in Melanoma. *Cell* **2012**, *150*, 251–263. [[CrossRef](#)] [[PubMed](#)]
25. Carvajal, R.D.; Antonescu, C.R.; Wolchok, J.D.; Chapman, P.B.; Roman, R.-A.; Teitcher, J.; Panageas, K.S.; Busam, K.J.; Chmielowski, B.; Lutzky, J.; et al. KIT as a Therapeutic Target in Metastatic Melanoma. *JAMA* **2011**, *305*, 2327–2334. [[CrossRef](#)]
26. Hribernik, A.; Cemazar, M.; Sersa, G.; Bosnjak, M.; Snoj, M. Effectiveness of electrochemotherapy after IFN- α adjuvant therapy of melanoma patients. *Radiol. Oncol.* **2016**, *50*, 21–27. [[CrossRef](#)]
27. Ray, A.; Williams, M.A.; Meek, S.M.; Bowen, R.C.; Grossmann, K.F.; Andtbacka, R.H.I.; Bowles, T.L.; Hyingstrom, J.R.; Leachman, S.A.; Grossman, D.; et al. A phase I study of intratumoral ipilimumab and interleukin-2 in patients with advanced melanoma. *Oncotarget* **2016**, *7*, 64390–64399. [[CrossRef](#)]
28. Venur, V.A.; Funchain, P.; Kotecha, R.; Chao, S.T.; Ahluwalia, M.S. Changing Treatment Paradigms for Brain Metastases from Melanoma-Part 1: Diagnosis, Prognosis, Symptom Control, and Local Treatment. *Oncology (Williston Park. N.Y.)* **2017**, *31*, 602–606.
29. Richtig, E.; Ludwig, R.; Kerl, H.; Smolle, J. Organ- and treatment-specific local response rates to systemic and local treatment modalities in stage IV melanoma. *Br. J. Dermatol.* **2005**, *153*, 925–931. [[CrossRef](#)]
30. Chang, M.Y.; McCannel, T. Local treatment failure after globe-conserving therapy for choroidal melanoma. *Br. J. Ophthalmol.* **2013**, *97*, 804–811. [[CrossRef](#)]
31. Stodell, M.; Thompson, J.; Emmett, L.; Uren, R.; Kapoor, R.; Saw, R. Melanoma patient imaging in the era of effective systemic therapies. *Eur. J. Surg. Oncol. (EJSO)* **2017**, *43*, 1517–1527. [[CrossRef](#)] [[PubMed](#)]
32. Menge, T.; Pellacani, G. Advances in noninvasive imaging of melanoma. *Semin. Cutan. Med. Surg.* **2016**, *35*, 18–24. [[CrossRef](#)] [[PubMed](#)]
33. Balasubramanya, R.; Selvarajan, S.K.; Cox, M.; Joshi, G.; Deshmukh, S.P.; Mitchell, D.G.; O’Kane, P. Imaging of ocular melanoma metastasis. *Br. J. Radiol.* **2016**, *89*, 20160092. [[CrossRef](#)] [[PubMed](#)]
34. Madu, M.; Wouters, M.W.; Van Akkooi, A. Sentinel node biopsy in melanoma: Current controversies addressed. *Eur. J. Surg. Oncol. (EJSO)* **2017**, *43*, 517–533. [[CrossRef](#)] [[PubMed](#)]
35. Walter, R.B.; Kazianis, S. Xiphophorus interspecies hybrids as genetic models of induced neoplasia. *ILAR J.* **2001**, *42*, 299–321. [[CrossRef](#)]
36. Egberts, F.; Hartje, C.; Schafmayer, C.; Kaehler, K.C.; Von Schönfels, W.; Hauschild, A.; Becker, T.; Egberts, J.H. Risk evaluation in cutaneous melanoma patients undergoing lymph node dissection: Impact of POSSUM. *Ann. R. Coll. Surg. Engl.* **2011**, *93*, 514–522. [[CrossRef](#)]
37. Giavazzi, R.; Decio, A. Syngeneic murine metastasis models: B16 melanoma. *Methods Mol. Biol.* **2014**, *1070*, 131–140.
38. Saleh, J. Murine models of melanoma. *Pathol. Res. Pract.* **2018**, *214*, 1235–1238. [[CrossRef](#)]
39. Nakamura, K.; Yoshikawa, N.; Yamaguchi, Y.; Kagota, S.; Shinozuka, K.; Kunitomo, M. Characterization of mouse melanoma cell lines by their mortal malignancy using an experimental metastatic model. *Life Sci.* **2002**, *70*, 791–798. [[CrossRef](#)]
40. Sadano, H.; Taniguchi, S.; Baba, T. Newly identified type of beta actin reduces invasiveness of mouse B16-melanoma. *FEBS Lett.* **1990**, *271*, 23–27. [[CrossRef](#)]
41. Shimokawa-Kuroki, R.; Sadano, H.; Taniguchi, S. A variant actin (beta m) reduces metastasis of mouse B16 melanoma. *Int. J. Cancer* **1994**, *56*, 689–697. [[CrossRef](#)]
42. Sadano, H.; Inoue, M.; Taniguchi, S. Differential Expression of Vinculin between Weakly and Highly Metastatic B16-Melanoma Cell Lines. *Jpn. J. Cancer Res.* **1992**, *83*, 625–630. [[CrossRef](#)] [[PubMed](#)]
43. Stei, M.M.; Loeffler, K.U.; Holz, F.G.; Herwig, M.C. Animal Models of Uveal Melanoma: Methods, Applicability, and Limitations. *BioMed Res. Int.* **2016**, *2016*, 1–9. [[CrossRef](#)] [[PubMed](#)]
44. Akimaru, K.; Stuhlmiller, G.M.; Seigler, H.F. Human melanoma growth in the peritoneal cavity of the athymic mouse—A model for in vivo study of cell-mediated immunity. *J. Surg. Oncol.* **1981**, *17*, 309–320. [[CrossRef](#)] [[PubMed](#)]
45. Zhao, Y.; Pang, B.; Detering, L.; Luehmann, H.; Yang, M.; Black, K.; Sultan, D.; Xia, Y.; Liu, Y. Melanocortin 1 Receptor Targeted Imaging of Melanoma With Gold Nanocages and Positron Emission Tomography. *Mol. Imaging* **2018**, *17*, 1536012118775827. [[CrossRef](#)] [[PubMed](#)]

46. Aasen, S.N.; Pospisilova, A.; Eichler, T.W.; Pánek, J.; Hruby, M.; Štěpánek, P.; Spriet, E.; Jirak, D.; Skaftnesmo, K.O.; Thorsen, F. A Novel Nanoprobe for Multimodal Imaging Is Effectively Incorporated into Human Melanoma Metastatic Cell Lines. *Int. J. Mol. Sci.* **2015**, *16*, 21658–21680. [[CrossRef](#)]
47. Zhao, Y.; Pang, B.; Luehmann, H.; Detering, L.; Yang, X.; Sultan, D.; Harpstrite, S.; Sharma, V.; Cutler, C.S.; Xia, Y.; et al. Gold Nanoparticles Doped with ¹⁹⁹Au Atoms and Their Use for Targeted Cancer Imaging by SPECT. *Adv. Health Mater.* **2016**, *5*, 928–935. [[CrossRef](#)]
48. Chen, J.; Shao, R.; Zhang, X.D.; Chen, C. Applications of nanotechnology for melanoma treatment, diagnosis, and theranostics. *Int. J. Nanomed.* **2013**, *8*, 2677–2688. [[CrossRef](#)]
49. Sahu, P.; Kashaw, S.; Sau, S.; Jain, S.; Jain, S.; Agrawal, R.K.; Iyer, A.K. pH Responsive 5-Fluorouracil Loaded Biocompatible Nanogels For Topical Chemotherapy of Aggressive Melanoma. *Colloids Surfaces B: Biointerfaces* **2019**, *174*, 232–245. [[CrossRef](#)]
50. Cheng, H.-B.; Sun, Z.; Kwon, N.; Wang, R.; Cui, Y.; Park, C.O.; Yoon, J. A Self-Assembled ATP Probe for Melanoma Cell Imaging. *Chem. Eur. J.* **2019**, *25*, 3501–3504. [[CrossRef](#)]
51. Cengelli, F.; Voinesco, F.; Juillerat-Jeanneret, L. Interaction of cationic ultrasmall superparamagnetic iron oxide nanoparticles with human melanoma cells. *Nanomed.* **2010**, *5*, 1075–1087. [[CrossRef](#)]
52. Pintaske, J.; Bantleon, R.; Kehlbach, R.; Claussen, C.D.; Wiskirchen, J.; Schick, F. Effect of Concentration of SH U 555A Labeled Human Melanoma Cells on MR Spin Echo and Gradient Echo Signal Decay at 0.2, 1.5, and 3T. *Magma Magn. Reson. Mater. Phys. Biol. Med.* **2006**, *19*, 71–77. [[CrossRef](#)] [[PubMed](#)]
53. Sundstrøm, T.; Daphu, I.; Wendelbo, I.; Hodneland, E.; Lundervold, A.; Immervoll, H.; Skaftnesmo, K.O.; Babic, M.; Jendelová, P.; Syková, E.; et al. Automated Tracking of Nanoparticle-labeled Melanoma Cells Improves the Predictive Power of a Brain Metastasis Model. *Cancer Res.* **2013**, *73*, 2445–2456. [[CrossRef](#)]
54. Vannucci, L.; Falvo, E.; Failla, C.M.; Carbo, M.; Fornara, M.; Canese, R.; Cecchetti, S.; Rajsiglova, L.; Stakheev, D.; Krizan, J.; et al. In Vivo Targeting of Cutaneous Melanoma Using an Melanoma Stimulating Hormone-Engineered Human Protein Cage with Fluorophore and Magnetic Resonance Imaging Tracers. *J. Biomed. Nanotechnol.* **2015**, *11*, 81–92. [[CrossRef](#)]
55. Hundt, W.; Steinbach, S.; Mayer, D.; Burbelko, M.; Kiessling, A.; Figiel, J.; Guccione, S. Magnetic resonance-imaging of the effect of targeted antiangiogenic gene delivery in a melanoma tumour model. *Eur. Radiol.* **2014**, *25*, 1107–1118. [[CrossRef](#)] [[PubMed](#)]
56. Schmieder, A.H.; Winter, P.M.; Caruthers, S.D.; Harris, T.D.; Williams, T.A.; Allen, J.S.; Lacy, E.K.; Zhang, H.; Scott, M.J.; Hu, G.; et al. Molecular MR imaging of melanoma angiogenesis with alphanubeta3-targeted paramagnetic nanoparticles. *Magn. Reson. Med.* **2005**, *53*, 621–627. [[CrossRef](#)] [[PubMed](#)]
57. Boles, K.S.; Schmieder, A.H.; Koch, A.W.; Carano, R.A.; Wu, Y.; Caruthers, S.D.; Tong, R.K.; Stawicki, S.; Hu, G.; Scott, M.J.; et al. MR angiogenesis imaging with Robo4- vs. alphaVbeta3-targeted nanoparticles in a B16/F10 mouse melanoma model. *FASEB J.* **2010**, *24*, 4262–4270. [[CrossRef](#)]
58. Baishya, R.; Nayak, D.K.; Kumar, D.; Sinha, S.; Gupta, A.; Ganguly, S.; Debnath, M.C. Ursolic Acid Loaded PLGA Nanoparticles: In vitro and in vivo Evaluation to Explore Tumor Targeting Ability on B16F10 Melanoma Cell Lines. *Pharm. Res.* **2016**, *33*, 2691–2703. [[CrossRef](#)]
59. Portilho, F.L.; Helal-Neto, E.; Cabezas, S.S.; Pinto, S.R.; Dos Santos, S.N.; Pozzo, L.; Sancenón, F.; Martínez-Máñez, R.; Santos-Oliveira, R. Magnetic core mesoporous silica nanoparticles doped with dacarbazine and labelled with ^{99m}Tc for early and differential detection of metastatic melanoma by single photon emission computed tomography. *Artif. Cells, Nanomedicine, Biotechnol.* **2018**, *46*, 1080–1087. [[CrossRef](#)]
60. Allen, K.J.H.; Jiao, R.; Malo, M.E.; Frank, C.; Fisher, D.R.; Rickles, D.; Dadachova, E. Comparative Radioimmunotherapy of Experimental Melanoma with Novel Humanized Antibody to Melanin Labeled with ²¹³Bismuth and ¹⁷⁷Lutetium. *Pharmaceutics* **2019**, *11*, 348. [[CrossRef](#)]
61. McCormack, D.R.; Bhattacharyya, K.; Kannan, R.; Katti, K.; Viator, J.A. Enhanced photoacoustic detection of melanoma cells using gold nanoparticles. *Lasers Surg. Med.* **2011**, *43*, 333–338. [[CrossRef](#)]
62. Shields, C.L.; Lim, L.-A.S.; Dalvin, L.A.; Shields, J.A. Small choroidal melanoma. *Curr. Opin. Ophthalmol.* **2019**, *30*, 206–214. [[CrossRef](#)] [[PubMed](#)]
63. Chen, F.; Zhang, X.; Ma, K.; Madajewski, B.; Benezra, M.; Zhang, L.; Phillips, E.; Turker, M.Z.; Gallazzi, F.; Penate-Medina, O.; et al. Melanocortin-1 Receptor-Targeting Ultrasmall Silica Nanoparticles for Dual-Modality Human Melanoma Imaging. *ACS Appl. Mater. Interfaces* **2018**, *10*, 4379–4393. [[CrossRef](#)] [[PubMed](#)]

64. Li, X.; Wang, D.; Ran, H.; Hao, L.; Cao, Y.; Ao, M.; Zhang, N.; Song, J.; Zhang, L.; Yi, H.; et al. A preliminary study of photoacoustic/ultrasound dual-mode imaging in melanoma using MAGE-targeted gold nanoparticles. *Biochem. Biophys. Res. Commun.* **2018**, *502*, 255–261. [[CrossRef](#)] [[PubMed](#)]
65. Chen, F.; Ma, K.; Zhang, L.; Madajewski, B.; Zanzonico, P.; Sequeira, S.; Gonen, M.; Wiesner, U.; Bradbury, M.S. Target-or-Clear Zirconium-89 Labeled Silica Nanoparticles for Enhanced Cancer-Directed Uptake in Melanoma: A Comparison of Radiolabeling Strategies. *Chem. Mater.* **2017**, *29*, 8269–8281. [[CrossRef](#)]
66. Balivada, S.; Rachakatla, R.S.; Wang, H.; Samarakoon, T.N.; Dani, R.K.; Pyle, M.; Kroh, F.O.; Walker, B.; Leaym, X.; Koper, O.B.; et al. A/C magnetic hyperthermia of melanoma mediated by iron(0)/iron oxide core/shell magnetic nanoparticles: A mouse study. *BMC Cancer* **2010**, *10*, 119. [[CrossRef](#)]
67. Zhao, J.; Zhang, Z.; Xue, Y.; Wang, G.; Cheng, Y.; Pan, Y.; Zhao, S.; Hou, Y. Anti-tumor macrophages activated by ferumoxytol combined or surface-functionalized with the TLR3 agonist poly (I:C) promote melanoma regression. *Theranostics* **2018**, *8*, 6307–6321. [[CrossRef](#)]
68. Tang, J.; Zhou, H.; Hou, X.; Wang, L.; Li, Y.; Pang, Y.; Chen, C.; Jiang, G.; Liu, Y. Enhanced anti-tumor efficacy of temozolomide-loaded carboxylated poly(amido-amine) combined with photothermal/photodynamic therapy for melanoma treatment. *Cancer Lett.* **2018**, *423*, 16–26. [[CrossRef](#)]
69. Tchounwou, C.; Sinha, S.S.; Nellore, B.P.V.; Pramanik, A.; Kanchanapally, R.; Jones, S.; Chavva, S.R.; Ray, P.C. Hybrid Theranostic Platform for Second Near-IR Window Light Triggered Selective Two-Photon Imaging and Photothermal Killing of Targeted Melanoma Cells. *ACS Appl. Mater. Interfaces* **2015**, *7*, 20649–20656. [[CrossRef](#)]
70. Harada, Y.; Ogawa, K.; Irie, Y.; Endo, H.; Feril, L.B.; Uemura, T.; Tachibana, K. Ultrasound activation of TiO₂ in melanoma tumors. *J. Control. Release* **2011**, *149*, 190–195. [[CrossRef](#)]
71. Vorobiof, D.; Rapoport, B.L.; Mahomed, R.; Karime, M. Phase II study of pegylated liposomal doxorubicin in patients with metastatic malignant melanoma failing standard chemotherapy treatment. *Melanoma Res.* **2003**, *13*, 201–203. [[CrossRef](#)] [[PubMed](#)]
72. Ascierto, P.A.; Marincola, F.M.; Atkins, M.B. What's new in melanoma? Combination! *J. Transl. Med.* **2015**, *13*, 213. [[CrossRef](#)]
73. Pollack, M.; Betof, A.; Dearden, H.; Rapazzo, K.; Valentine, I.; Brohl, A.; Ancell, K.; Long, G.; Menzies, A.; Eroglu, Z.; et al. Safety of resuming anti-PD-1 in patients with immune-related adverse events (irAEs) during combined anti-CTLA-4 and anti-PD1 in metastatic melanoma. *Ann. Oncol.* **2018**, *29*, 250–255. [[CrossRef](#)] [[PubMed](#)]
74. Tran, M.A.; Smith, C.D.; Kester, M.; Robertson, G.P. Combining Nanoliposomal Ceramide with Sorafenib Synergistically Inhibits Melanoma and Breast Cancer Cell Survival to Decrease Tumor Development. *Clin. Cancer Res.* **2008**, *14*, 3571–3581. [[CrossRef](#)]
75. Pegoraro, C.; Cecchin, D.; Gracia, L.S.; Warren, N.; Madsen, J.; Armes, S.P.; Lewis, A.; MacNeil, S.; Battaglia, G. Enhanced drug delivery to melanoma cells using PMPC-PDPA polymersomes. *Cancer Lett.* **2013**, *334*, 328–337. [[CrossRef](#)] [[PubMed](#)]
76. Hartono, S.B.; Yu, M.; Gu, W.; Yang, J.; Strounina, E.; Wang, X.; Qiao, S.; Yu, C. Synthesis of multi-functional large pore mesoporous silica nanoparticles as gene carriers. *Nanotechnology* **2014**, *25*, 55701. [[CrossRef](#)]
77. Pang, B.; Zhao, Y.; Luehmann, H.; Yang, X.; Detering, L.; You, M.; Zhang, C.; Zhang, L.; Li, Z.-Y.; Ren, Q.; et al. 64Cu-Doped PdCu@Au Tripods: A Multifunctional Nanomaterial for Positron Emission Tomography and Image-Guided Photothermal Cancer Treatment. *ACS Nano* **2016**, *10*, 3121–3131. [[CrossRef](#)]
78. Mishra, H.; Mishra, P.; Iqbal, Z.; Jaggi, M.; Madaan, A.; Bhuyan, K.; Gupta, N.; Gupta, N.; Vats, K.; Verma, R.; et al. Co-Delivery of Eugenol and Dacarbazine by Hyaluronic Acid-Coated Liposomes for Targeted Inhibition of Survivin in Treatment of Resistant Metastatic Melanoma. *Pharmaceutics* **2019**, *11*, 163. [[CrossRef](#)]
79. Blanco, E.; Shen, H.; Ferrari, M. Principles of nanoparticle design for overcoming biological barriers to drug delivery. *Nat. Biotechnol.* **2015**, *33*, 941–951. [[CrossRef](#)]
80. Greish, K.; Nehoff, H.; Parayath, N.N.; Domanovitch, L.; Taurin, S. Nanomedicine for drug targeting: Strategies beyond the enhanced permeability and retention effect. *Int. J. Nanomed.* **2014**, *9*, 2539–2555. [[CrossRef](#)]
81. Durymanov, M.; Kamaletdinova, T.; Lehmann, S.E.; Reineke, J. Exploiting passive nanomedicine accumulation at sites of enhanced vascular permeability for non-cancerous applications. *J. Control. Release* **2017**, *261*, 10–22. [[CrossRef](#)]

82. Heo, G.S.; Zhao, Y.; Sultan, D.; Zhang, X.; Detering, L.; Luehmann, H.P.; Zhang, X.; Li, R.; Choksi, A.; Sharp, S.; et al. Assessment of Copper Nanoclusters for Accurate in Vivo Tumor Imaging and Potential for Translation. *ACS Appl. Mater. Interfaces* **2019**, *11*, 19669–19678. [[CrossRef](#)] [[PubMed](#)]
83. DeNardo, G.L.; Natarajan, A.; Hok, S.; Mirick, G.; DeNardo, S.J.; Corzett, M.; Sysko, V.; Lehmann, J.; Beckett, L.; Balhorn, R. Nanomolecular HLA-DR10 Antibody Mimics: A Potent System for Molecular Targeted Therapy and Imaging. *Cancer Biotherapy Radiopharm.* **2008**, *23*, 783–795. [[CrossRef](#)]
84. Ahamed, M.; Alhadlaq, H.; Alam, J.; Khan, M.A.M.; Ali, D.; Alarafi, S. Iron oxide nanoparticle-induced oxidative stress and genotoxicity in human skin epithelial and lung epithelial cell lines. *Curr. Pharm. Des.* **2013**, *19*, 6681–6690. [[CrossRef](#)] [[PubMed](#)]
85. Majzoub, R.N.; Ewert, K.K.; Safinya, C.R. Cationic liposome–nucleic acid nanoparticle assemblies with applications in gene delivery and gene silencing. *Philos. Trans. R. Soc. A: Math. Phys. Eng. Sci.* **2016**, *374*, 20150129. [[CrossRef](#)] [[PubMed](#)]
86. Canli, E.G.; Ila, H.B.; Canli, M. Responses of biomarkers belonging to different metabolic systems of rats following oral administration of aluminium nanoparticle. *Environ. Toxicol. Pharmacol.* **2019**, *69*, 72–79. [[CrossRef](#)]

Publisher's Note: MDPI stays neutral with regard to jurisdictional claims in published maps and institutional affiliations.



© 2020 by the authors. Licensee MDPI, Basel, Switzerland. This article is an open access article distributed under the terms and conditions of the Creative Commons Attribution (CC BY) license (<http://creativecommons.org/licenses/by/4.0/>).